J|A|C|S
ARTICLES
Published on Web 03/09/2004

Probing Slow Dynamics in High Molecular Weight Proteins by Methyl-TROSY NMR Spectroscopy: Application to a 723-Residue Enzyme

Dmitry M. Korzhnev, Karin Kloiber, Voula Kanelis, Vitali Tugarinov, and Lewis E. Kay*

Contribution from the Protein Engineering Network Centres of Excellence and the Departments of Medical Genetics, Biochemistry, and Chemistry, University of Toronto, Toronto, Ontario, Canada M5S 1A8

Received November 13, 2003; E-mail: kay@pound.med.utoronto.ca

Abstract: A new CPMG-based multiple quantum relaxation dispersion experiment is presented for measuring millisecond dynamic processes at side-chain methyl positions in high molecular weight proteins. The experiment benefits from a methyl-TROSY effect in which cancellation of intramethyl dipole fields occurs, leading to methyl $^{13}C-^{1}H$ correlation spectra of high sensitivity and resolution (Tugarinov, V.; Hwang, P. M.; Ollerenshaw, J. E.; Kay, L. E. *J. Am. Chem. Soc.* **2003**, *125*, 10420−10428). The utility of the methodology is illustrated with an application to a highly deuterated, methyl-protonated sample of malate synthase G, an 82 kDa enzyme consisting of a single polypeptide chain. A comparison of the sensitivity obtained using the present approach relative to existing HSQC-type ^{13}C single quantum dispersion experiments shows a gain of a factor of 5.4 on average, significantly increasing the range of applications for this methodology.

Introduction

One of the important goals of chemical biology is to relate molecular structure to biological function, and there is an increasingly large number of examples where this has been achieved.[1] For many systems, however, the static three-dimensional pictures produced by X-ray diffraction or NMR spectroscopy fall short of explaining function, since they do not take into account dynamic features which are often a prerequisite for activity.[2] NMR spectroscopy is a particularly powerful technique for studying site-specific dynamics over a wide range of time scales involving a large number of probes and can potentially bridge the gap between structure and an understanding of function in cases where dynamics are critical.[3,4]

A potential drawback associated with the application of NMR spectroscopy to many biological systems of interest, however, relates to the size limitations of the technique. Many important systems have molecular weights that are in excess of 30−40 kDa, currently the upper limit of most applications, and may therefore not be amenable to study using existing methodology. The development of transverse relaxation optimized spectroscopy (TROSY) has significantly impacted the range of problems that can be studied with NMR.[5] Particularly relevant to the work reported here are experiments by Palmer and co-workers[6] and Kempf et al.[7] involving TROSY versions of ^{15}N Carr−Purcell−Meiboom−Gill[8,9] (CPMG)- and spin-lock-based relaxation dispersion experiments that extend the study of slow (microsecond−millisecond) dynamic processes at backbone protein sites to higher molecular weight systems. A complementary experiment for measuring slow motions at side-chain methyl sites would be of substantial interest since the dynamics of methyls can often report on the hydrophobic interior of proteins. We have recently shown that it is possible to record $^{13}C-^{1}H$ correlation maps of methyl groups in highly deuterated proteins by exploiting a TROSY effect in which cancellation of dipole fields significantly enhances spectral sensitivity and resolution.[10]

Here we present an experiment for studying millisecond dynamics at methyl side-chain positions in large proteins, based on this principle, in which the relaxation of $^{13}C-^{1}H$ multiple quantum coherence is measured during a fixed CPMG delay. Several advantages over ^{13}C single quantum dispersion profiles have emerged. First, sensitivity gains using the new methodology are critical, with enhancements on the order of a factor of 5 for the application considered here. Second, the dispersion profiles thus obtained are sensitive to both ^{13}C *and* ^{1}H chemical

(1) Stryer, L. *Biochemistry*, 4th ed.; W. H. Freeman: New York, 1995.
(2) Alber, T.; Gilbert, W. A.; Ponzi, D. R.; Petsko, G. A. *Ciba Found. Symp.* **1983**, *93*, 4−24.
(3) Mulder, F. A. A.; Mittermaier, A.; Hon, B.; Dahlquist, F. W.; Kay, L. E. *Nat. Struct. Biol.* **2001**, *8*, 932−935.
(4) Eisenmesser, E. Z.; Bosco, D. A.; Akke, M.; Kern, D. *Science* **2002**, *295*, 1520−1523.
(5) Pervushin, K.; Riek, R.; Wider, G.; Wüthrich, K. *Proc. Natl. Acad. Sci. U.S.A.* **1997**, *94*, 12366−12371.
(6) Loria, J. P.; Rance, M.; Palmer, A. G. *J. Biomol. NMR* **1999**, *15*, 151−155.
(7) Kempf, J. G.; Jung, J.; Sampson, N. S.; Loria, J. P. *J. Am. Chem. Soc.* **2003**, *125*, 12064−12065.
(8) Carr, H. Y.; Purcell, E. M. *Phys. Rev.* **1954**, *4*, 630−638.
(9) Meiboom, S.; Gill, D. *Rev. Sci. Instrum.* **1958**, *29*, 688−691.
(10) Tugarinov, V.; Hwang, P.; Ollerenshaw, J.; Kay, L. E. *J. Am. Chem. Soc.* **2003**, *125*, 10420−10428.

10.1021/ja039587i CCC: $27.50

shift differences between exchanging sites, unlike ^{13}C single quantum profiles which depend only on differences in carbon shifts. In favorable cases, both ^{13}C and ^{1}H shift differences can be extracted from fits of multiple quantum dispersions. The utility of the present approach is illustrated with an application to the 82 kDa single polypeptide chain enzyme, malate synthase G[11] (MSG), 37 °C (correlation time, τ_C, of 45 ns in D_2O), confirming the benefits of the methodology.

Materials and Methods

Sample Preparation. A U-[^{15}N,^{2}H], Ileδ1-[^{13}C,^{1}H] sample of MSG was obtained as described in detail previously[10] using U-[^{2}H]-glucose (CIL, Andover, MA) and $^{15}NH_4Cl$ (CIL, Andover, MA) as the carbon and nitrogen sources, respectively, with the addition of 100 mg of 4-[^{13}C,^{1}H]-3,3-^{2}H-α-ketobutyrate to the 1 L growth medium 1 h prior to induction. The sample of U-[^{15}N,^{2}H], Leu-[$^{13}CH_3$,$^{12}CD_3$], Val-[$^{13}CH_3$,$^{12}CD_3$] MSG was obtained in a similar fashion except that 100 mg of 2-keto-3-methyl-d_3-3-d_1-4-^{13}C-butyrate (α-ketoisovalerate deuterated at the β-position and with one of the two methyl groups $^{13}CH_3$ and the other $^{12}CD_3$; all other positions deuterated) was used as a precursor.[12] The 3,3-[^{1}H] positions of protonated α-ketobutyrate, purchased from Isotec (Miamisburg, OH), were quantitatively exchanged to ^{2}H by incubation of a 2.7 mM solution of the compound in 99.9% D_2O at 45 °C, pH 10.5 (uncorrected) for 20 h, following the procedure of Gardner et al.[13] The sodium salt of 2-keto-3-methyl-d_3-4-^{13}C-butyrate was custom synthesized at Isotec (Miamisburg, OH), and the 3-[^{1}H] position was exchanged to ^{2}H by incubation of a 25 mM solution in 99.9% D_2O at 45 °C, pH 12.4 (uncorrected) for 3 h, as described by Goto et al.[14] Both reactions were followed to completion by ^{1}H NMR.

NMR Spectroscopy. All dispersion profiles were recorded on samples that were 0.7 mM in protein, 100% D_2O, 25 mM sodium phosphate, pH 7.1, 20 mM $MgCl_2$, 0.05% NaN_3, 0.1 mg/mL Pefabloc, and 5 mM DTT at field strengths of 600 and 800 MHz using the pulse sequence of Figure 1. In the case of the Ile-protonated sample, dispersions were recorded at both 37 and 5 °C with the ^{13}C carrier placed at 13.9 ppm. ν_{cpmg} values ($1/(4\delta)$, where 2δ is the spacing between successive 180° pulses) ranging from 25 Hz (100 Hz) to 1 kHz were used for the Ile sample at 37 °C (5 °C) along with a T value of 40 (10) ms; 28 (37 °C) and 12 (5 °C) ν_{cpmg} values were recorded per dispersion along with three duplicates to assess the experimental errors. Data sets with acquisition times of [73 ms, 64 ms] ([44 ms, 64 ms]) in [t_1, t_2] were obtained at 37 °C (5 °C), along with 8(48) scans per FID and repetition delays of 1.5 s, giving rise to acquisition times on the order of 20(28) h per dispersion at 600 MHz (25% longer at 800 MHz). Dispersions at 37 °C were obtained for the Leu,Val protonated sample with ν_{cpmg} values ranging from 50 Hz to 1 kHz (15 values), $T = 20$ ms, and the ^{13}C carrier positioned at 23 ppm. Data sets with acquisition times of [64 ms, 64 ms] in [t_1, t_2] were obtained, with 16 scans per FID (using a delay between scans of 1.5 s) for an acquisition time of 30 h per dispersion (600 MHz).

Data sets were processed using NMRPipe/NMRDraw software[15] and analyzed using in-house written programs. Cross-peak intensities were obtained by three-way decomposition of a 3D data set consisting of a series of dispersion spectra recorded as a function of ν_{cpmg} using the MUNIN approach.[16,17] Values of $R_{2,eff}$ were calculated for each CPMG frequency (see below) from the relation $R_{2,eff} = -1/T \ln\{I(\nu_{cpmg})/I(0)\}$, where $I(\nu_{cpmg})$ and $I(0)$ are the intensities of cross-peaks recorded with and without the interval T, respectively. Errors for $R_{2,eff}$ values were estimated from repeat measurements, as described previously.[18] In cases where calculated errors were less than 2% of the $R_{2,eff}$ rate, a value of 2% was used.

As described above, a pair of MSG samples (U-[^{15}N,^{2}H], Ileδ1-[^{13}C,^{1}H] and U-[^{15}N,^{2}H], Leu-[$^{13}CH_3$,$^{12}CD_3$],Val-[$^{13}CH_3$,$^{12}CD_3$]) has been used to obtain dispersion data. An advantage of using the pair of samples described above is that by minimizing the number of protons, the remaining methyls have more favorable relaxation properties. This is particularly the case for Ile residues. For example, multiple quantum Ileδ1 T_2 values of 58 ± 20 and 44 ± 16 ms were obtained for U-[^{15}N,^{2}H], Ileδ1-[^{13}C,^{1}H] and U-[^{15}N,^{2}H], Ileδ1-[^{13}C,^{1}H], Leu-[$^{13}CH_3$,$^{12}CD_3$],Val-[$^{13}CH_3$,$^{12}CD_3$] MSG samples, respectively,[12] leading to higher quality dispersions from Ile residues in the selectively labeled Ile sample. We have, however, recently demonstrated that high quality methyl-TROSY spectra can be recorded using a single U-[^{15}N,^{2}H], Ileδ1-[^{13}C,^{1}H], Leu-[$^{13}CH_3$,$^{12}CD_3$],Val-[$^{13}CH_3$,$^{12}CD_3$] labeled preparation[12] so that a complete set of dispersions involving Ile, Leu, and Val can be obtained on a single sample. However, in applications to large proteins such as MSG where sensitivity is critical we prefer to record dispersions using the pair of samples described above.

Of note, extensive simulations have shown that multiple quantum dispersion profiles are more sensitive to pulse offset effects than experiments based on single quantum coherences. To give a "feel" for the sort of errors that are involved, we consider a two-site exchange process with separation between ^{13}C and ^{1}H chemical shifts in the two states of 1 and 0 ppm, respectively, $k_{ex} = 1000\ s^{-1}$, and a relative population of the major form of 95% ($R_{2,eff}$(50 Hz) − $R_{2,eff}$(1000 Hz) ≈ 30 s^{-1}). The average pairwise rmsd between $R_{2,eff}$ values calculated for a ^{13}C offset of 5 ppm (800 MHz static field) and a (homogeneous) ^{13}C B_1 field of 14 kHz and $R_{2,eff}$ values calculated assuming on-resonance pulses is less than 1 s^{-1} for $0 \le \nu_{cpmg} \le 1$ kHz (although larger errors in individual $R_{2,eff}$ values can be obtained), with considerably smaller rmsd values for B_1 fields of 20 kHz. Calculations have been repeated taking into account, in addition, the spatial inhomogeneity of the B_1 field. With the B_1 field distribution on our probe (measured using the procedure of Desvaux and co-workers[19]) and for the exchange parameters and offsets listed above, errors in $R_{2,eff}$ that are very similar to those quoted above are obtained (i.e., the effects of inhomogeneity are small). Depending on the size of the dispersions and the errors that can be tolerated, it will very likely be prudent to record separate profiles for Ile and for Leu/Val methyls with the carrier placed in the center of the regions of interest in both cases (using as high a B_1 field as possible), thereby minimizing the effects of finite pulse widths.

Results and Discussion

Experimental Scheme. Figure 1 shows the pulse scheme for measuring $^{13}C-^{1}H$ multiple quantum relaxation dispersion profiles of methyl groups in proteins. The experiment is derived from an HMQC sequence[20,21] that is particularly advantageous for recording methyl correlations in methyl-protonated, highly deuterated samples of high molecular weight proteins.[10] Very recently, it was demonstrated that $^{13}C-^{1}H$ correlation spectra recorded with the HMQC scheme can be as much as a factor of 3 more sensitive than corresponding HSQC data sets and that the origin of the sensitivity enhancement is a methyl-

(11) Howard, B. R.; Endrizzi, J. A.; Remington, S. J. *Biochemistry* **2000**, *39*, 3156−68.
(12) Tugarinov, V.; Kay, L. E. *J. Biomol. NMR* **2004**, *28*, 165−172.
(13) Gardner, K. H.; Kay, L. E. *J. Am. Chem. Soc.* **1997**, *119*, 7599−7600.
(14) Goto, N. K.; Gardner, K. H.; Mueller, G. A.; Willis, R. C.; Kay, L. E. *J. Biomol. NMR* **1999**, *13*, 369−374.
(15) Delaglio, F.; Grzesiek, S.; Vuister, G. W.; Zhu, G.; Pfeifer, J.; Bax, A. *J. Biomol. NMR* **1995**, *6*, 277−293.
(16) Orekhov, V. Y.; Ibraghimov, I. V.; Billeter, M. *J. Biomol. NMR* **2001**, *20*, 49−60.
(17) Korzhnev, D. M.; Ibraghimov, I. V.; Billeter, M.; Orekhov, V. Y. *J. Biomol. NMR* **2001**, *21*, 263−268.
(18) Mulder, F. A. A.; Hon, B.; Mittermaier, A.; Dahlquist, F. W.; Kay, L. E. *J. Am. Chem. Soc.* **2002**, *124*, 1443−1451.
(19) Guenneugues, M.; Berthault, P.; Desvaux, H. *J. Magn. Reson.* **1999**, *136*, 118−126.
(20) Bax, A.; Griffey, R. H.; Hawkings, B. L. *J. Magn. Reson.* **1983**, *55*, 301−315.
(21) Mueller, L. *J. Am. Chem. Soc.* **1979**, *101*, 4481−4484.

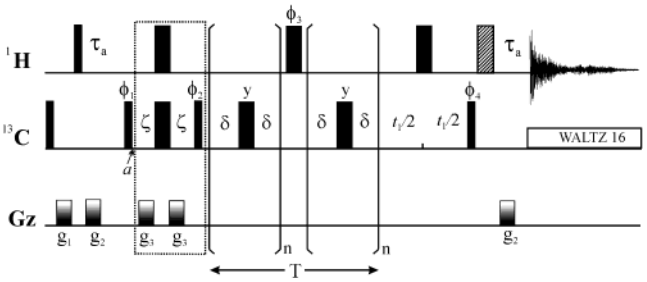

Figure 1. Pulse scheme of the methyl-TROSY ^{13}C−^{1}H multiple quantum relaxation dispersion experiment. For applications involving proteins where methyl lines L1 and L3 decay rapidly to zero, the purge element in the dashed box can be eliminated, and the ^{1}H 180° hatched pulse is employed. All of the dispersion profiles recorded for MSG were not obtained with the purge element; however, in hindsight we recommend using the purge for all applications since it ensures that L1 = L3 = 0 at $T = 0$, which can be beneficial for residues with very high mobility (see text). For smaller proteins, the purge element is required (tumbling times less than approximately 12 ns), and the hatched proton pulse eliminated. Half of the ^{1}H 180° pulse width is subtracted from the δ periods immediately preceding and following the pulse of phase $\phi 3$. Intensities, $I(0)$, are measured by removing all elements during the interval T with the exception of the 180° pulse of phase $\phi 3$. All 90° (180°) pulses are indicated by narrow (wide) rectangles and are applied along the x-axis, unless indicated otherwise; the ^{1}H pulse in the center of t_1 is of the composite variety[34] ($90_x180_y90_x$). ^{1}H and ^{13}C carriers are positioned in the center of the region of interest (1 ppm for ^{1}H, 13.9 ppm for Ile, and 23 ppm for Leu/Val). All proton pulses are employed with the highest possible r.f. power, while ^{13}C pulses with a field strength of ~19 kHz are recommended (a lower field, 13 kHz was used in the applications here). ^{13}C decoupling during acquisition is achieved using a 1.5−2.0 kHz WALTZ-16 field.[35] The delays used are $\tau_a = 3.6$ ms, $2\zeta = 2.0$ ms. The constant time delay, T, is typically set so that approximately 50% of the signal decays in this interval; values used in the applications discussed here are listed in Materials and Methods. Quadrature is achieved via states-TPPI of phase $\phi 4$.[36] The phase cycle employed is: $\phi 1 = x, -x$; $\phi 3 = 2(x), 2(y), 2(-x), 2(-y)$; $\phi 4 = x$; rec = $(x, -x, -x, x)$ when the purge is omitted and $\phi 1 = x, -x$; $\phi 2 = 2(y), 2(-y)$, $\phi 3 = 4(x), 4(y)$; $\phi 4 = x$; rec = $2(x, -x), 2(-x, x)$ when the purge is included. The durations and strengths of the gradients (z-axis) are: $g1$ = (1 ms, 5 G/cm), $g2$ = (0.6 ms, 20 G/cm), and $g3$ = (0.2 ms, −20 G/cm).

TROSY effect involving the cancellation of intramethyl dipolar interactions.[10] Briefly, it can be shown that for an isolated methyl group tumbling in the macromolecular limit and assuming rapid methyl rotation the methyl coherences that contribute to observed correlations in both HSQC and HMQC spectra relax in a single exponential manner with either fast or slow time constants.[22−26] Remarkably, in the HMQC experiment two separate coherence transfer pathways contribute to the observed signal: one where the relaxation rates of the operative coherences are slow and a second involving only the fast relaxing elements. For applications involving high molecular weight proteins, such as MSG (see below), the latter pathway does not contribute to the detected signal since the decay for the fast relaxing coherences throughout the pulse scheme is extensive. The HMQC sequence ensures that the slowly relaxing transitions are not interconverted with the fast relaxing components, thus preserving 50% of the signal. In contrast, in the HSQC scheme substantial mixing occurs during the transfer of magnetization from ^{1}H to ^{13}C and back to ^{1}H, so that fast and slowly relaxing elements are interconverted, leading to significant losses in sensitivity and resolution.

At point *a* in the sequence of Figure 1 an equal superposition of double and zero quantum ^{13}C−^{1}H coherences are created, $2C_YI_X$ (neglecting ^{1}H chemical shift evolution) where C_Y and I_X denote the Y and X components of ^{13}C and ^{1}H magnetization, respectively (referred to in what follows as multiple quantum coherence). A ^{13}C CPMG pulse train is applied during the subsequent constant time interval, T (the scheme in the dashed box is described later), with a ^{1}H 180° pulse at the center to refocus ^{1}H chemical shift evolution during this period. Following the delay T, ^{13}C chemical shift evolution is recorded during t_1, and magnetization is transferred back to protons for observation. The experiment is repeated with different delays between ^{13}C refocusing pulses and the effective decay rate calculated as $R_{2,\mathrm{eff}} = -1/T \ln\{I(\nu_{\mathrm{cpmg}})/I(0)\}$, where $\nu_{\mathrm{cpmg}} = 1/(4\delta)$ and 2δ is the spacing between successive 180° pulses and $I(\nu_{\mathrm{cpmg}})$ and $I(0)$ are the intensities of cross-peaks recorded with and without the interval T, respectively.

It can be shown[10,27] that the coherence of interest at point *a*, $2C_YI_X$, is given by $2C_YI_{X,1} + 2C_YI_{X,2} + 2C_YI_{X,3}$, with $2C_YI_{X,i} = 2C_YI_{X,i}\{|\beta\beta><\beta\beta| + |\alpha\beta><\alpha\beta| + |\beta\alpha><\beta\alpha| + |\alpha\alpha><\alpha\alpha|\}$, where $\{\alpha,\beta\}$ are spin states of methyl protons $j,k \in (1,2,3)$ and $i \neq j \neq k$. Insight into how $2C_YI_X$ evolves can be obtained by focusing on each of the three elements L1 = $\sum 2C_YI_{X,i}\{|\beta\beta><\beta\beta|\}$, L2 = $\sum 2C_YI_{X,i}\{|\alpha\beta><\alpha\beta| + |\beta\alpha><\beta\alpha|\}$, and L3 = $\sum 2C_YI_{X,i}\{|\alpha\alpha><\alpha\alpha|\}$, since these elements give rise to the components that make up the observed correlations in HMQC maps.[10,27] The sums in L1, L2, and L3 are over the index i. In a simple HMQC scheme where the effects of chemical shift evolution are neglected and where the ^{1}H refocusing pulse is eliminated from the t_1 evolution period, a 1(L1):2(L2):1(L3) triplet is observed, assuming that each of the lines relaxes with the same time constant. For macromolecules, such as MSG, however, L1 and L3 decay very rapidly and only L2 contributes to the observed signal.[10,27] For applications where the decay of L1 and L3 is not sufficiently rapid so that L1, L2, and L3 are present throughout the course of the pulse scheme of Figure 1, the purge element in the dashed box is employed to eliminate L1 and L3. This element includes an interval $2\zeta = 1/(4\,J_{\mathrm{CH}})$, where J_{CH} is the one-bond ^{13}C−^{1}H coupling constant, during which time the outer lines, L1 and L3, evolve due to scalar coupling to become orthogonal with respect to L2 (which does not evolve due to J_{CH}). These lines are subsequently eliminated by the action of the ^{13}C $90_{\phi 2}$ pulse and its phase cycle.

Theoretical Considerations Involving ^{13}C−^{1}H Multiple Quantum Dispersions. At first glance it might be tempting to conclude that the attenuation of signal during the T delay resulting from chemical exchange follows the same functional dependence that would be observed if dispersion profiles of single quantum ^{13}C coherences were to be recorded, since in both cases essentially identical CPMG elements are used. However, multiple quantum coherences are present during the CPMG interval in the present experiment, with interconversion between double and zero quantum elements afforded by the ^{13}C 180° pulses applied during this period. The resulting dispersion profiles are sensitive to differences in *both* ^{1}H and ^{13}C chemical shifts of exchanging states in a manner that, in some cases, allows both shift differences to be extracted. Although the

(22) Tugarinov, V.; Kay, L. E. *J. Mol. Biol.* **2003**, *327*, 1121−1133.
(23) Muller, N.; Bodenhausen, G.; Ernst, R. R. *J. Magn. Reson.* **1987**, *75*, 297−334.
(24) Kay, L. E.; Prestegard, J. H. *J. Am. Chem. Soc.* **1987**, *109*, 3829−3835.
(25) Kay, L. E.; Torchia, D. A. *J. Magn. Reson.* **1991**, *95*, 536−547.
(26) Werbelow, L. G.; Marshall, A. G. *J. Magn. Reson.* **1973**, *11*, 299−313.
(27) Ollerenshaw, J. E.; Tugarinov, V.; Kay, L. E. *Magn. Reson. Chem.* **2003**, *41*, 843−852.

analysis is slightly more complex than that for single quantum[28] or individual double or zero quantum dispersion profiles,[29] the advantage of extracting both ^{1}H and ^{13}C shift differences (e.g., in cases with large $\Delta\omega_H$; see below) is significant, and the sensitivity gains associated with the multiple quantum experiment relative to ^{1}H and ^{13}C single quantum schemes are critical.

The multiple quantum element present immediately prior to the T period, L2, consists of both double and zero quantum ^{13}C−^{1}H coherences, in equal amounts. It can be shown that the decay of the signal over the CPMG interval of duration T in a two-site exchanging system is given by the rate, $R_{2,\mathrm{eff}}$:

$$-(1/T)\ln\left\{\mathrm{Re}\left(\frac{0.5}{p_A}[1\ 0](\boldsymbol{AB}+\boldsymbol{CD})\begin{bmatrix}p_A\\p_B\end{bmatrix}\right)\right\} \tag{1}$$

where p_A and p_B are the populations of the major and minor conformers, respectively, and the matrixes $\boldsymbol{A}$, $\boldsymbol{B}$, $\boldsymbol{C}$, and $\boldsymbol{D}$ are given, in turn, by

$$\boldsymbol{A}=(\boldsymbol{M_1M_2M_2M_1})^{n/2},\ \boldsymbol{B}=(\boldsymbol{M_2^*M_1^*M_1^*M_2^*})^{n/2}$$
$$\boldsymbol{C}=(\boldsymbol{M_2M_1M_1M_2})^{n/2},\ \boldsymbol{D}=(\boldsymbol{M_1^*M_2^*M_2^*M_1^*})^{n/2}$$

for even n and by

$$\begin{aligned}\boldsymbol{A}&=(\boldsymbol{M_1M_2M_2M_1})^{(n-1)/2}\boldsymbol{M_1M_2},\\ \boldsymbol{B}&=(\boldsymbol{M_1^*M_2^*M_2^*M_1^*})^{(n-1)/2}\boldsymbol{M_1^*M_2^*}\\ \boldsymbol{C}&=(\boldsymbol{M_2M_1M_1M_2})^{(n-1)/2}\boldsymbol{M_2M_1},\\ \boldsymbol{D}&=(\boldsymbol{M_2^*M_1^*M_1^*M_2^*})^{(n-1)/2}\boldsymbol{M_2^*M_1^*}*\end{aligned} \tag{2.1}$$

for odd n, where $\boldsymbol{M_j}=\exp(\boldsymbol{m_j}\delta)$, $j=1,2$, the superscript * denotes complex conjugate, and

$$\boldsymbol{m_1}=\begin{pmatrix}-p_Bk_{ex}-R_{2,DQ}^A & p_Ak_{ex}\\ p_Bk_{ex} & -p_Ak_{ex}-i(\Delta\omega_H+\Delta\omega_C)-R_{2,DQ}^B\end{pmatrix}$$
$$\boldsymbol{m_2}=\begin{pmatrix}-p_Bk_{ex}-R_{2,ZQ}^A & p_Ak_{ex}\\ p_Bk_{ex} & -p_Ak_{ex}-i(\Delta\omega_H-\Delta\omega_C)-R_{2,ZQ}^B\end{pmatrix} \tag{2.2}$$

In eq 2, $\boldsymbol{M_1}$ and $\boldsymbol{M_2}$ are the appropriate evolution matrixes for double and zero quantum coherences, respectively, p_Bk_{ex} (p_Ak_{ex}) is the rate constant for the exchange from site A to B (B to A), $\Delta\omega_C$ and $\Delta\omega_H$ are the differences in methyl ^{13}C and ^{1}H chemical shifts (rad/s) between states A and B, respectively, and $R_{2,DQ}$ (double quantum) and $R_{2,ZQ}$ (zero quantum) are the transverse relaxation rates for L2 in the absence of exchange, with the superscript A,B denoting the site. In what follows we have assumed that the relaxation properties in both sites are identical in the absence of exchange. Thus, the effective intrinsic relaxation rate over the complete CPMG element is $R_{2,MQ}=1/2(R_{2,DQ}+R_{2,ZQ})$. We have fit the experimental data numerically to extract the relevant exchange parameters, $\Delta\omega_C$, $\Delta\omega_H$, p_B ($=1-p_A$), and k_{ex}, along with $R_{2,MQ}$ at each static magnetic field. Note that in the limit that $\Delta\omega_H=0$, eq 2 equally well describes the evolution of ^{13}C single quantum magnetization that exchanges between a pair of sites.

As will be discussed in detail elsewhere, it is also possible to derive an analytical expression, much like the Carver−Richards formula,[30,31] which gives the relation between $R_{2,\mathrm{eff}}$ and $\nu_{cpmg}=1/(4\delta)$:

$$R_{2,\mathrm{eff}}\left(\frac{1}{2\delta}\right)=\mathrm{Re}(\lambda_1)-\frac{1}{4n\delta}\ln(Q) \tag{3.1}$$

with

$$\lambda_1=R_{2,MQ}+\frac{1}{2}\left(k_{ex}-\frac{1}{2\delta}\cosh^{-1}(D_+\cosh\eta_+-D_-\cos\eta_-)\right) \tag{3.2}$$

$$D_\pm=\frac{1}{2}\left(\frac{\Psi+2\Delta\omega_C{}^2}{\sqrt{\Psi^2+\zeta^2}}\pm 1\right) \tag{3.3}$$

$$\eta_\pm=\sqrt{2}\delta\sqrt{\sqrt{\Psi^2+\zeta^2}\pm\Psi} \tag{3.4}$$

$$\Psi=(i\Delta\omega_H+(p_A-p_B)k_{ex})^2-\Delta\omega_C{}^2+4p_Ap_Bk_{ex}{}^2 \tag{3.5}$$

$$\zeta=-2\Delta\omega_C(i\Delta\omega_H+(p_A-p_B)k_{ex}) \tag{3.6}$$

and with

$$Q=\mathrm{Re}(1-m_D{}^2+m_Dm_Z-m_Z{}^2+(1/2)(m_D+m_Z)\sqrt{p_B/p_A}) \tag{3.7}$$

$$m_D=\frac{ik_{ex}\sqrt{p_Ap_B}}{d_+z_+}\left(z_++2\Delta\omega_C\frac{\sin(z_+\delta)}{\sin((d_++z_+)\delta)}\right) \tag{3.8}$$

$$m_Z=-\frac{ik_{ex}\sqrt{p_Ap_B}}{d_-z_-}\left(d_--2\Delta\omega_C\frac{\sin(d_-\delta)}{\sin((d_-+z_-)\delta)}\right) \tag{3.9}$$

$$d_\pm=(\Delta\omega_H+\Delta\omega_C)\pm ik_{ex},\ z_\pm=(\Delta\omega_H-\Delta\omega_C)\pm ik_{ex} \tag{3.10}$$

Equation 3.1 can be recast as $I(\nu_{cpmg})=I(0)Q\exp(-\mathrm{Re}(\lambda_1)4n\delta)$ ($T=4n\delta$), where Q is a function of ν_{cpmg} but not n. Note that λ_1 is a complex number whose imaginary part approaches zero as $\Delta\omega_H\rightarrow 0$. In this limit, $\mathrm{Re}(\lambda_1)$ is equal to the Carver−Richards expression that is routinely used to fit dispersion data derived from single quantum coherences. Of interest, although $\ln(Q)$ is small, it does not go to zero in the limit that $\Delta\omega_H\rightarrow 0$, and the dependence of $R_{2,\mathrm{eff}}$ ($=-(1/T)\ln(I(\nu_{cpmg})/I(0))$ on ν_{cpmg} should be fit using eq 3.1 and not $\mathrm{Re}(\lambda_1)$ in the case that a constant time CPMG period is used (although for T values greater than ~30 ms any errors that arise from fitting with $\mathrm{Re}(\lambda_1)$, at least for dispersions from single quantum coherences, will be small and likely within noise). In contrast, if dispersion experiments are conducted in a nonconstant time manner by measuring the decay of signal for several T values at a given ν_{cpmg} (and subsequently repeating the process for different ν_{cpmg} values), $R_{2,\mathrm{eff}}(1/(2\delta))$ is defined by the slope of $\ln(I(T))$ vs T, given by $\mathrm{Re}(\lambda_1)$.

(28) Palmer, A. G.; Kroenke, C. D.; Loria, J. P. *Methods Enzymol.* **2001**, *339*, 204−238.
(29) Orekhov, V. Y.; Korzhnev, D. M.; Kay, L. E. *J. Am. Chem. Soc.* **2004**, *126*, 1886−1891.
(30) Carver, J. P.; Richards, R. E. *J. Magn. Reson.* **1972**, *6*, 89−105.
(31) Jen, J. *J. Magn. Reson.* **1978**, *30*, 111−128.

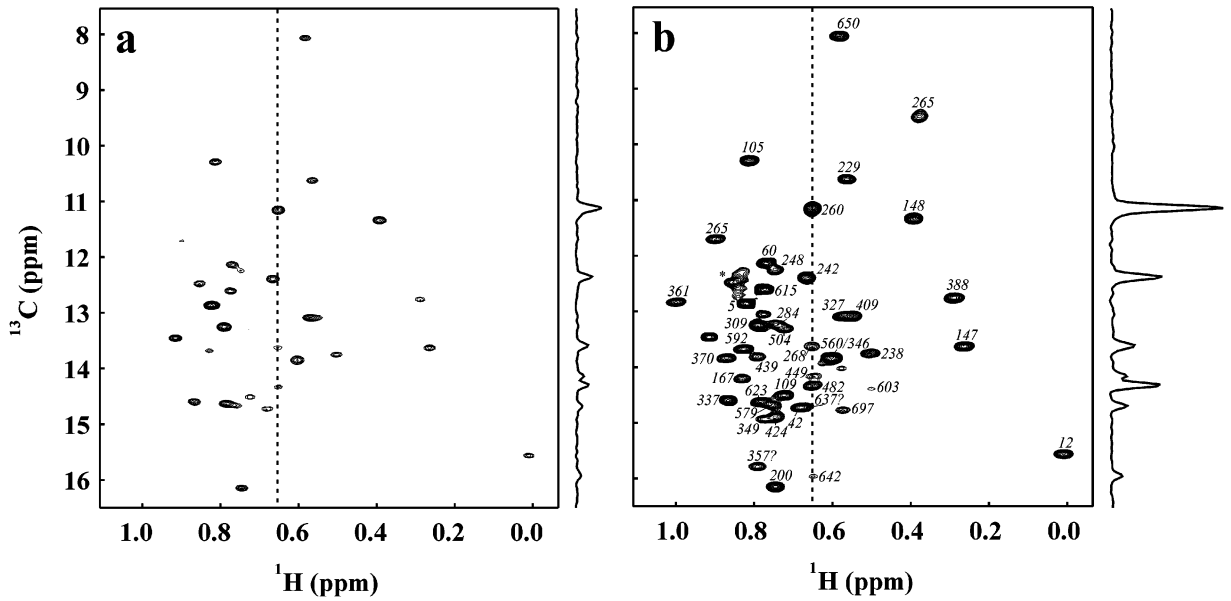

Figure 2. Comparison of ^{13}C−^{1}H correlation maps recorded (a) with the sequence of Skrynnikov et al.[32] and (b) with the scheme of Figure 1 using a U-[^{15}N,^{2}H], Ileδ1-[^{13}C,^{1}H] MSG sample, 37 °C, 600 MHz with $T = 40$ ms and $\nu_{cpmg} = 1$ kHz. Both data sets are plotted at the same noise level so that the relative sensitivity of the experiments can be assessed visually. A trace at $F_2 = 0.63$ ppm is indicated along the sides of each of the data sets. Ileδ1 methyl assignments are listed in *b* (two of the Ileδ1 methyls are tentatively assigned and are indicated with "?"). The peak labeled * likely arises from a slight amount of protein degradation.

The extra dependence on $\Delta\omega_H$ (see eq 2, 3), relative to the case for exchange involving single quantum magnetization, introduces a number of interesting features into the dispersion profiles that will be discussed in detail in a subsequent publication. Most notable is that $R_{2,eff}$ values can actually increase as a function of ν_{cpmg} for some exchange processes in the slow to intermediate regime. For example, consider the case of a two-site slow exchange process, $k_{ex} \ll \Delta\omega$, with $\Delta\omega_C = \Delta\omega_H$ ($\Delta\varpi_C = (\gamma_H/\gamma_C)\Delta\varpi_H$; in what follows ω is in units of rad/s, while ϖ is the equivalent in ppm). In the slow pulsing limit ($\delta \rightarrow \infty$), the contribution to $R_{2,eff}$ (site A) from exchange ($R_{2,eff}(0)$) is $k_{AB}/2$, where the factor of 2 takes into account the fact that double and zero quantum coherences are present for equal amounts of time during the course of the CPMG period and that only double quantum coherences are affected by exchange (when $\Delta\omega_C = \Delta\omega_H$, see eq 2). In contrast, in the fast pulsing limit the contribution to relaxation from exchange due to differences in ^{13}C chemical shifts between states is quenched, and the exchange process is equivalent to one in which only proton single quantum magnetization interconverts between states. There is thus a contribution to $R_{2,eff}$ ($R_{2,eff}(\infty)$) of k_{AB}. It follows, therefore, that $R_{2,eff}(\infty) > R_{2,eff}(0)$, and dispersions that increase with ν_{cpmg} are obtained.

Sensitivity Considerations. Prior to recording dispersion profiles of MSG, we first established that significant improvements in sensitivity using methyl-TROSY spectroscopy could be obtained relative to an approach developed previously by Skrynnikov et al.,[32] which relies on the establishment of HSQC-type coherences. Figure 2 shows a comparison of data sets recorded on a U-[^{15}N,^{2}H], Ileδ1-[^{13}C,^{1}H] sample of MSG with identical acquisition parameters, at 37 °C, with $T = 40$ ms, and $\nu_{cpmg} = 1$ kHz. In Figure 2, both data sets are plotted at the same noise level, and it is clear that the sensitivity of the spectrum recorded with the scheme of Figure 1 (Figure 2b) is far superior. On average, a 5.4-fold gain in signal-to-noise is obtained, with individual values ranging from 1.8 to 9.7-fold. Cross sections at $F_2 = 0.63$ ppm (indicated by dashed lines) are shown to the right of each data set.

Flat Dispersions Are Obtained in the Absence of Exchange. As an additional test of the methodology, we were interested in ensuring that the dispersion profiles obtained report faithfully on the chemical dynamics of the system without complications from the spin physics inherent to the methyl probes that we were using. Note that in the absence of exchange, flat dispersion profiles would be expected, and therefore, the presence of artificial dispersion profiles must result from spin−spin interactions associated with the methyl probe. For example, simulations have shown that spin flips involving external proton spins can give rise to dispersion profiles that are indistinguishable from those generated due to chemical exchange. In practice, the spin flip rate can be minimized by recording spectra on highly deuterated proteins with selective methyl protonation;[10,12] in the present study we have employed U-[^{15}N,^{2}H], Ileδ1-[^{13}C,^{1}H], and U-[^{15}N,^{2}H], Leu-[^{13}CH$_3$,^{12}CD$_3$], Val-[^{13}CH$_3$,^{12}CD$_3$] samples of malate synthase G. The average value for $\xi = (\sum_i(1/r_{HHi}^6))^{-1/6}$ for each Ile methyl proton in the protein (where the sum is over all external protons *Hi*), calculated from the X-ray structure of the glyoxylate-bound form of the protein,[11] varies between 2.5 and 11 Å (average of 5.5 Å). Average ξ values of 3.7 and 4.0 are obtained for the corresponding distances for Leu and Val methyls in the L,V-labeled sample described above.

Figure 3a shows dispersion profiles recorded with the scheme of Figure 1 (purge element in dashed box not used) for a number of Ile, Leu, and Val methyl groups in MSG with small ξ values (<3 Å). In all cases, reasonably flat dispersion profiles are

(32) Skrynnikov, N. R.; Mulder, F. A. A.; Hon, B.; Dahlquist, F. W.; Kay, L. E. *J. Am. Chem. Soc.* **2001**, *123*, 4556−4566.

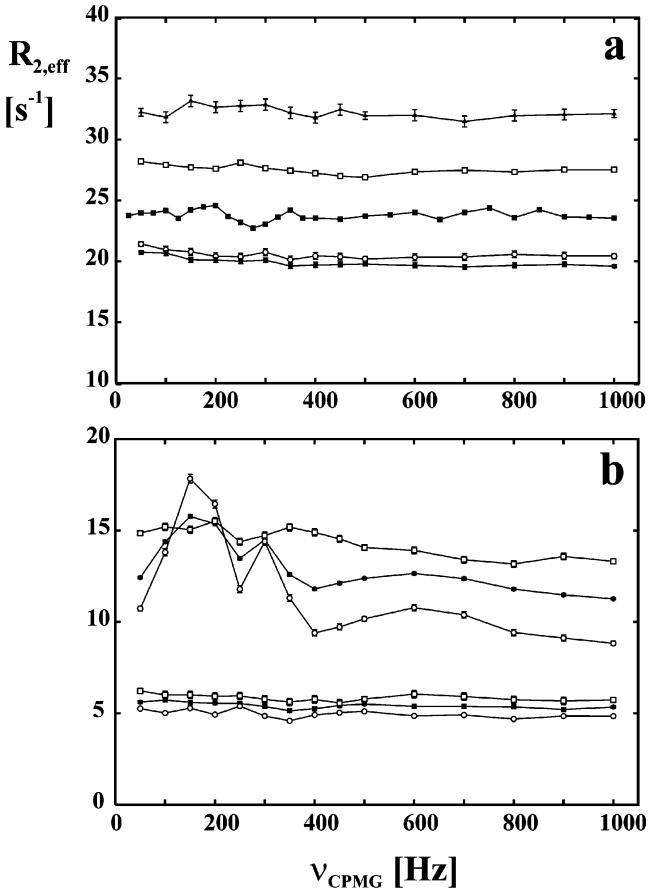

Figure 3. (a) Dispersion profiles recorded at 600 MHz, 37 °C, for selected methyls of MSG with effective distances to neighboring protons, ξ, less than 3 Å. The pulse sequence in Figure 1, without the purge element, was employed using a B_1 field strength of 13 kHz for ^{13}C pulses. Dispersions from Leu 572 ($\xi = 2.9$ Å), Val 275 ($\xi = 2.7$ Å), Ile 349($\xi = 3.0$ Å), Val 100 ($\xi = 2.9$ Å), and Leu 174 ($\xi = 2.9$ Å) are illustrated (in order of increasing $R_{2,eff}(\infty)$), showing that spin flip effects are minimal for the labeling scheme employed. Note that stereospecific assignments are not presently available for Leu and Val methyls and that the distances reported are the smallest of each methyl pair calculated for each Leu/Val residue. (b) Dispersion profiles recorded for selected methyls from protein L (600 MHz, 25 °C) using the scheme of Figure 1 without (upper three traces) and with the purge element (bottom three traces). Dispersions for Leu 8δ1, Ile 4δ1, and Leu 56δ2 are indicated with open circles, closed squares, and open squares, respectively. The offsets from the carbon carrier are 1060, −1080, and 650 Hz for Leu 8δ1, Ile 4δ1, and Leu 56δ2, respectively (^{13}C B_1 field of 13 kHz). Only when the outer lines are purged (for protein L at 25 °C) are flat dispersions obtained.

obtained, and in none of the cases would the profiles generated be confused with those reflecting chemical exchange processes. Although the experiments were performed on a pair of samples, with protonation confined to Ile (Ile dispersions) or Leu/Val ([$^{13}CH_3$,$^{12}CD_3$]; Leu/Val dispersions), spin flips would not be expected to interfere with the extraction of accurate exchange parameters from fits of dispersions measured on a single U-[^{15}N,^{2}H], Ileδ1-[^{13}C,^{1}H], Leu-[$^{13}CH_3$,$^{12}CD_3$], Val-[$^{13}CH_3$,$^{12}CD_3$] sample of MSG. In the case of Leu and Val, ξ decreases to 3.5 Å, on average, for a U-[^{15}N,^{2}H], Ileδ1-[^{13}C,^{1}H], Leu-[$^{13}CH_3$,$^{12}CD_3$], Val-[$^{13}CH_3$,$^{12}CD_3$] MSG sample (close to 4 Å for samples with [$^{13}CH_3$,$^{12}CD_3$] labeling at Leu and Val and with Ile fully deuterated), while a large decrease for Ile is noted relative to preparations where Ile Cδ1 is selectively protonated (from 5.5 to 3.5 Å). These average values are, however, still larger than the values of ξ for the residues that are illustrated in Figure 3a, for which relatively flat dispersion curves were measured. The results obtained experimentally are consistent with those generated with simulations showing that for the majority of ξ values found in highly deuterated samples with Ile, Leu, and Val methyl protonation of the type described above, reasonably flat dispersion profiles are expected (data not shown).

Of interest, simulations further establish that the purge element of Figure 1 that eliminates L1 and L3 immediately prior to the start of the T period does help minimize the effects of spin flips, even when such effects are small to begin with. As the average value of ξ increases and for applications involving high molecular weight samples that are highly deuterated and labeled as described in Materials and Methods (such as MSG, $\xi_{min} = 2.4$ Å), with L1 and L3 decaying rapidly, the purge element becomes less important and has not been used in any of the experiments involving MSG in the present study. However, in very pathological cases, for a very mobile residue (methyl axis order parameter squared of 0.2), with $\xi = 2$ Å for example, simulations do show that the purge element can be very beneficial in attenuating contributions to dispersion curves that would otherwise arise from spin flips, even in studies involving large proteins.

We have also prepared a U-[^{15}N,^{2}H], Ileδ1-[^{13}C,^{1}H], Leu-[$^{13}CH_3$,$^{12}CD_3$], Val-[$^{13}CH_3$,$^{12}CD_3$] sample of protein L (63 residues) to evaluate the utility of the methodology for applications to small proteins. Figure 3b illustrates a number of profiles obtained from an application to protein L, 25 °C. This protein has been studied extensively in our laboratory, and it has been established that millisecond time scale dynamics are not present, so that flat dispersions are anticipated. The upper three traces show the profiles measured for Leu 8δ1 (open circles), Ile 4δ1 (closed squares), and Leu 56δ2 (open squares) using the sequence of Figure 1, without the purge element (dashed box). The profiles for Leu 8δ1 and Ile 4δ1 are particularly bad for low ν_{cpmg} values, with $R_{2,eff}$ varying by as much as 7 s^{-1} between points. Dispersion profiles of the sort illustrated by the upper traces in Figure 3b are not the result of spin flips involving external protons, since such effects would then be observed in profiles from MSG. Moreover, these profiles can be reproduced by computations that do not include relaxation. Density matrix simulations show that dispersion profiles from methyls with substantial ^{13}C chemical shift offsets will not be flat and will have the appearance observed experimentally for Leu 8 and Ile 4 (offsets of 1060 and −1080 Hz, respectively, ^{13}C B_1 field strength of 13 kHz) in applications involving small proteins, such as protein L (overall tumbling time of 5 ns in D_2O, 25 °C). Although modest improvements can be obtained using stronger B_1 fields and employing composite pulse schemes, the profiles are still unsatisfactory. Simulations establish that at the heart of the problem is the accumulation of coherences originating from L1 and L3 during the first half of the CPMG scheme that are subsequently not refocused by the ^{1}H 180° pulse in the center of the period and the ensuing pulse train. These terms arise due to the combined effect of pulse imperfections and evolution due to both J_{CH} and chemical shift. Not surprisingly, therefore, flat dispersions are obtained when J_{CH} is set to zero in the computations. Experimentally, these artifacts can be eliminated by purging the outer lines (L1, L3 above), so that magnetization from only the middle element (L2) remains. The boxed element in Figure 1 illustrates the simple purge element

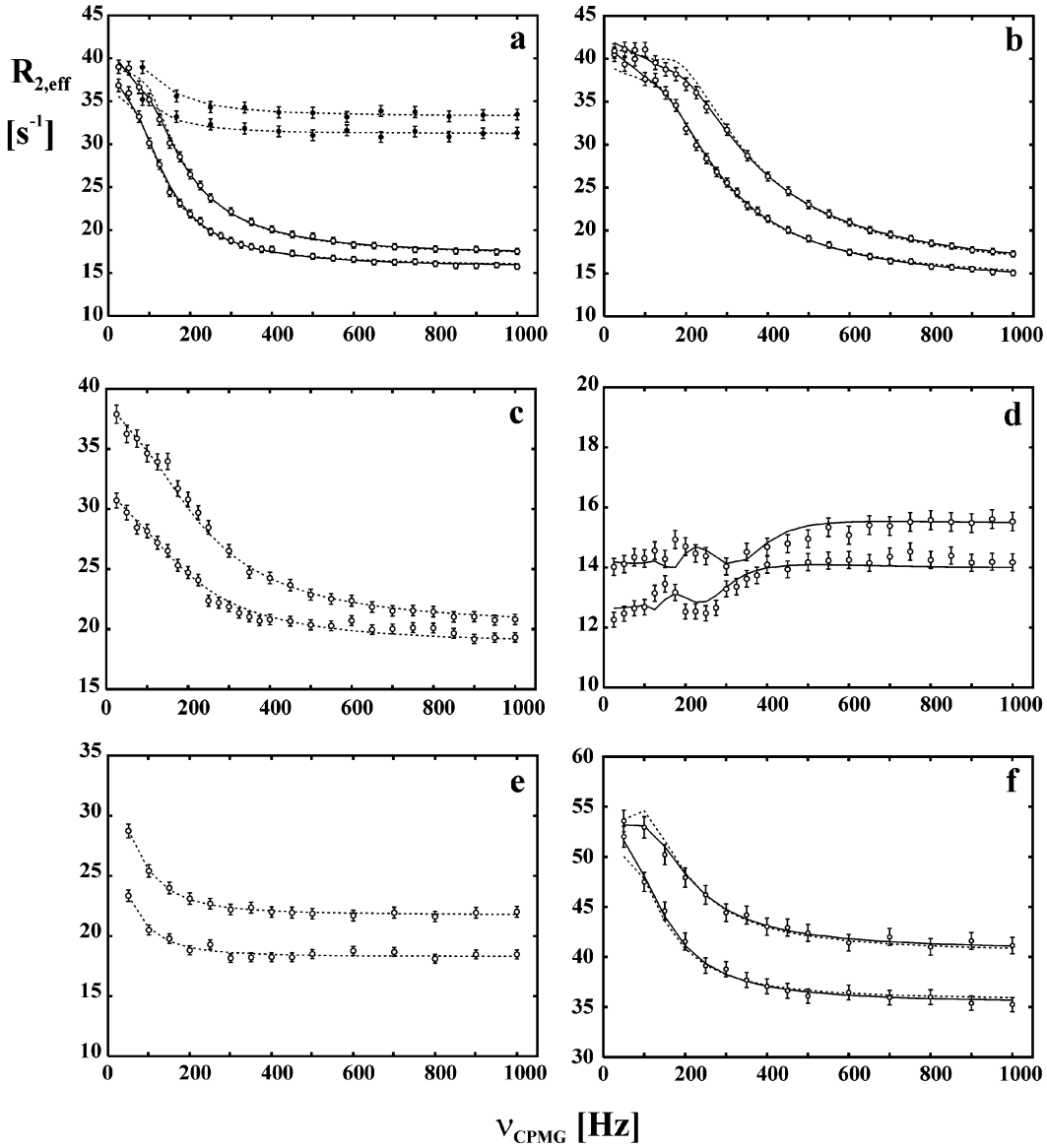

Figure 4. Selected dispersion profiles for Ile, Leu, and Val residues in MSG, 37 °C, recorded at 600 and 800 MHz, as described in Materials and Methods (upper profile is the one recorded at 800 MHz). Profiles of methyls from Ile 242, 260, 424, and 42 are illustrated in parts a−d, respectively, with curves for methyls from Val 189 and Leu 128 indicated in e and f. In the case of Ile 242, profiles obtained at 5 °C are also shown, with 2 s^{-1} added to $R_{2,eff}$ values recorded at 800 MHz. (Dispersion profiles for the other residues at 5 °C are not available due to overlap and slight shifts of cross-peaks relative to 37 °C, which made it difficult to definitively assign correlations at the lower temperature based on the assignments obtained at 37 °C.) The dashed lines are obtained from fits where $\Delta\varpi_H$ is set to zero, with the solid lines generated from fits where $\Delta\varpi_H$ is allowed to vary (eqs 1 and 2). Solid lines are only shown where statistically significant improvements in fits with variable $\Delta\varpi_H$ are obtained. Details of data fitting and extracted exchange parameters are given in Supporting Information.

that is employed, described above. The bottom three profiles in Figure 3b show dispersions (B_1 field for the ^{13}C refocusing pulses of 13 kHz) from the same three methyls, recorded now using the scheme of Figure 1 with the purge element. Flat dispersions are obtained, with $R_{2,eff}$ rates that are considerably reduced, since only the slowly relaxing L2 component (and not L1 or L3) contributes to the resultant signal. We note in passing that all of the dispersions in protein L, including those originating from methyls with small ξ values, are flat (when the purge element is employed), as expected for samples that employ the labeling scheme detailed above. Finally, we have recorded dispersions of protein L using the scheme of Figure 1 without the purge element over a range of temperatures to establish what the effective overall tumbling time is where lines L1 and L3 decay sufficiently so that flat dispersions are obtained without purging. We find that for correlation times exceeding approximately 12 ns the purge element is not necessary. All of the ensuing applications involving MSG were obtained, therefore, using the scheme of Figure 1 without the purge element.

Slow Dynamics in MSG. Satisfied that the methodology developed is superior to our previous scheme in the case of applications involving high molecular weight proteins and that artifacts due to proton spin flips will be minimal, we subsequently recorded dispersion experiments on MSG at fields of 600 and 800 MHz (see Materials and Methods). Figure 4a−f shows a number of dispersion profiles from Ile, Leu, and Val methyls of the protein. We have fit the dispersion curves numerically to eqs 1 and 2 above, both with $\Delta\varpi_H = 0$ (dashed lines, model 1) and with $\Delta\varpi_H$ variable (solid lines, model 2).

Dispersions indicated only with dashed lines are those for which fits using variable $\Delta\varpi_H$ values were no better than when $\Delta\varpi_H$ was set to 0 ppm, established on the basis of F-test statistical analyses. The fitting procedure, including the statistical criteria used to distinguish between the two models, and a list of the extracted exchange parameters is presented in Supporting Information. It is worth reiterating here that multiple quantum dispersions are more sensitive to pulse offset effects than their single quantum analogues, especially for low ν_{CPMG} values, and therefore, it may be difficult to distinguish between cases where $\Delta\varpi_H = 0$ from those for which $\Delta\varpi_H$ is very small on the basis of any statistical criteria. In this regard, reduced χ^2 values less than 1 are obtained from fits of dispersions from all but one of the residues listed in Supporting Information Table 1 (but not Supporting Information Table 2; see below) using *either* models 1 or 2.

Initial studies made use of a U-[^{15}N,^{2}H], Ileδ1-[^{13}C,^{1}H] sample of MSG in D_2O, which was available from our previous work, and dispersions were obtained at 37 °C ($\tau_C = 45$ ns) and 5 °C ($\tau_C = 118$ ns). Dispersions from Ile 242 at 37 °C (open circles) and at 5 °C (closed circles) are illustrated in Figure 4a. Interestingly, the sums of the forward and reverse rates, k_{ex}, are similar at the two temperatures (400 ± 20 s^{-1}, 37 °C and 310 ± 150 s^{-1}, 5 °C), as are the ^{13}C shift differences between the ground and excited states (0.7 ± 0.03 and 0.6 ± 0.1 ppm). In contrast, the population of the excited state, p_B, decreases from 9.6 ± 0.6 (37 °C) to 2.3 ± 0.6% (5 °C), accounting for the significantly smaller exchange contribution to relaxation observed at the lower temperature. Of note, the best fits for the data at 37 °C (5 °C), which are statistically significant, give $\Delta\varpi_H = 0.05$ ppm (0 ppm).

Dispersion profiles for Ile 260, 37 °C are shown in Figure 4b. Better fits (F-test statistics) are obtained with a model in which $\Delta\varpi_H$ is allowed to vary ($\Delta\varpi_H = 0.08$ ppm), solid line, relative to the case where $\Delta\varpi_H$ is fixed to zero. Figure 4c illustrates profiles for Ile 424, 37 °C. The k_{ex} values of the Ile residues highlighted in Figure 4a−c nearly span the range of rates that we have observed in MSG, from approximately 200 to 1100 s^{-1} (see Supporting Information). Figure 4d illustrates a pair of dispersion profiles from Ile 42, 37 °C, that could only be fit with an appreciable $\Delta\varpi_H$ value (0.4 ppm), and in this case $R_{2,eff}$(1000 Hz) > $R_{2,eff}$(25 Hz). The signal-to-noise of correlations from this residue in the dispersion spectra is sufficiently high that the "fine structure" expected in the dispersion profile (note the oscillations around 200 Hz in the fitted, theoretical curves) can be observed in the experimental data. Other residues for which $R_{2,eff}$(1000 Hz) > $R_{2,eff}$(25 Hz) are listed in Supporting Information. We have obtained dispersions of the type illustrated in Figure 4d for five out of a total of 44 Ile in the protein (~10%). For these residues, $0.45\Delta\omega_H \le \Delta\omega_C$ (rad/s) $\le 1.6\Delta\omega_H$, with $\Delta\varpi_H \ge 0.14$ ppm and $|R_{ex}| \le 2$ s^{-1} (800 MHz; see Supporting Information). Such small dispersions can be quantified in these cases because of the high sensitivity of the experiments and, most important, the small intrinsic transverse relaxation rates of these residues. Of note, we have not observed dispersions for any Leu or Val which are of the type illustrated for Ile 42, Figure 4d. In general, errors in $R_{2,eff}$ for the dispersions from Leu/Val are larger than for Ile since (i) the intrinsic relaxation rates of Leu and Val (samples where Leu and Val methyls are [$^{13}CH_3$,$^{12}CD_3$]) are higher than that for Ile (samples where only Ile is protonated) and (ii) the effective concentration of Leu/Val methyls is half that of Ile due to the labeling scheme that we have implemented (see below).

The success of initial measurements involving Ile probes of dynamics in MSG prompted the consideration of additional methyl groups. Methyls of Leu and Val were selected since robust approaches for preparing highly deuterated Leu, Val methyl-protonated proteins have been described in the literature using methyl-protonated isovalerate as a precursor.[14] Since the quality of methyl correlations in HMQC spectra decreases with increasing proton density,[10,12] a sample was prepared in which only one methyl in Leu and Val each was of the $^{13}CH_3$ variety, with the second $^{12}CD_3$, using a $^{13}CH_3$,$^{12}CD_3$ isovalerate precursor[12] (see Materials and Methods). This significantly reduces contributions to relaxation from external protons, leading to spectra of much higher sensitivity and resolution than would otherwise be obtained with samples containing [$^{13}CH_3$,$^{13}CH_3$]-labeled Leu, Val.[10,12] Notably, a factor of 2(1.6) increase in sensitivity was obtained in correlation maps recorded with the sequence of Figure 1, $T = 40(20)$ ms, 37 °C for MSG samples with Val and Leu residues consisting of a single $^{13}CH_3$ group relative to the corresponding sample with both methyls protonated. The gain in sensitivity occurs despite the fact that the effective concentration of methyls is twice as high in the latter sample. Moreover, the reduced proton density is important for minimizing methyl spin flips as discussed above (ξ_{av} of 3.9 and 2.4 Å in [$^{13}CH_3$,$^{12}CD_3$] and [$^{13}CH_3$,$^{13}CH_3$] samples, respectively), leading to an increase in the accuracy of the extracted exchange parameters. We would, therefore, *not recommend* recording dispersions on U-[^{15}N,^{2}H], Leu-[$^{13}CH_3$,$^{13}CH_3$], Val-[$^{13}CH_3$,$^{13}CH_3$] samples. Parts e and f of Figure 4 show a pair of dispersion profiles (600 and 800 MHz) obtained for methyls from Val 189 and Leu 128, measured on a U-[^{15}N,^{2}H], Leu-[$^{13}CH_3$,$^{12}CD_3$], Val-[$^{13}CH_3$,$^{12}CD_3$] sample of MSG in D_2O at 37 °C. Even for residues with large $R_{2,eff}(\infty)$ values, such as Leu 128 (~40 s^{-1}, Figure 4f; or for Leu 142, ~50 s^{-1}, not shown), it is still possible to obtain quantifiable dispersion profiles, although the errors are often somewhat larger than for residues with more favorable intrinsic relaxation properties.

As described above, the dispersions in Figure 4 were fit to models with $\Delta\varpi_H = 0$ (model 1) and with $\Delta\varpi_H \neq 0$ (model 2). Residues I242 (37 °C), I260, I42, and L128 of Figure 4 were best fit with model 2, although a comparison of the fits (solid and dashed lines in the Figure) shows that the differences between the two models can be subtle. In this regard, we have noted that there can be some interplay between values of p_B, $\Delta\varpi_H$, $\Delta\varpi_C$, and $R_{2,eff}(\infty)$ obtained in some of the fits with model 2, with large values for p_B and correspondingly smaller values for $\Delta\varpi_C$ and $R_{2,eff}(\infty)$ generated with the more complex model (see Supporting Information). In these cases, the exchange parameters must be interpreted cautiously. Whenever possible, we recommend measuring single quantum ^{13}C dispersions and performing a "joint" analysis of single and multiple quantum data sets; simultaneous fits to a combination of ^{13}C single and ^{1}H−^{13}C multiple quantum profiles minimize the interplay discussed above. Unfortunately, in the present application to MSG the sensitivity of the ^{13}C single quantum experiment precludes such an analysis.

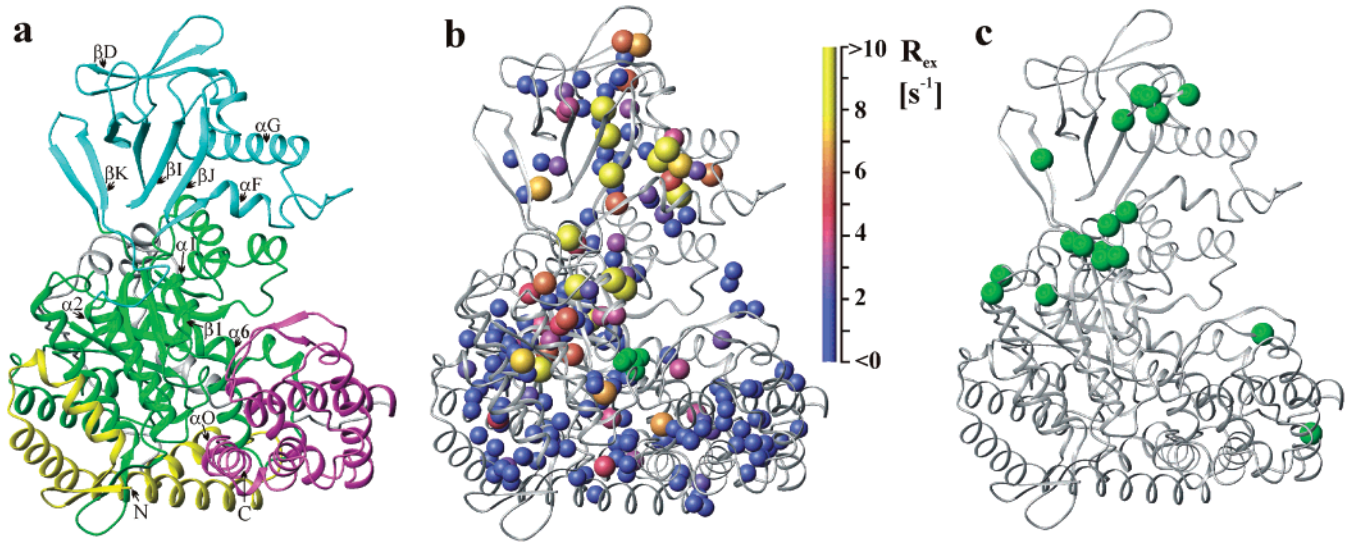

Figure 5. (a) Ribbon diagram of the glyoxylate-bound form of MSG (PDB coordinates 1d8c),[11] with the four domains of the enzyme color-coded. (b) Methyl groups for which dispersion data have been obtained at 37 °C are indicated by spheres, color- and size-coded, to show the amount of R_{ex} at 800 MHz (larger spheres more exchange). N- and C-termini of the protein are indicated by N and C, respectively. Glyoxylate is shown in green in b. Since at present there are no stereospecific assignments for the methyls of Val and Leu, R_{ex} values for these residues are assigned arbitrarily to each of the two methyls. (c) Backbone ^{15}N amides for which dispersion profiles with R_{ex}(800 MHz) $\geq$ 5 s^{-1} have been measured, 37 °C. The diagrams were generated using Molmol.[37]

The examples illustrated in Figure 4 clearly indicate that, at least in the cases where dispersions are large, slow time scale processes can be quantified in high molecular weight proteins. Recall that the correlation times of MSG (in D_2O) at 37 and 5 °C are 45 ns and ~120 ns, respectively,[10] and that previous backbone ^{15}N spin relaxation experiments have established that each of the four domains of the enzyme tumbles with the same correlation time, reflecting the overall rotation of the protein.[33] That dispersions can be recorded with high sensitivity on systems of this size and in proteins where the domains are not "beads on a string" but tightly interacting entities, opens the possibility for studying slow time scale dynamics at methyl sites in many important biological systems.

Figure 5a shows a ribbon diagram of MSG, based on the X-ray structure of the glyoxylate-bound form of the protein[11] (the apo-form is studied here), with the four domains of the molecule color-coded. At the core of the structure is a β8/α8 barrel domain (green) from which the other domains extend. This domain is flanked on one side by the N-terminal α-helical clasp (yellow) and on the opposite side by an α/β domain (blue). The C-terminal end of the enzyme consists of a five-helix plug (pink), connected to the barrel by a loop−helix−turn−helix−loop structure (shown in gray in the figure). Interestingly, we have recently established that, in contrast to what was expected on the basis of an analysis of other functionally and structurally related enzymes, the relative orientation of the domains does not change upon ligand binding.[22] Thus, it is of interest to investigate whether the linker regions between domains, in particular, are flexible on the millisecond time scale.

^{13}C relaxation dispersion profiles have been measured for 42 well resolved and assigned Ile δ1 and 189 Val γ1/γ2 and Leu δ1/δ2 resonances, corresponding to 84% of the Ile, Leu, and Val methyl groups in the protein. Figure 5b shows the spatial arrangement of the methyls, with exchange contributions, R_{ex}, to the transverse relaxation rates, $R_{2,eff}$, measured at 800 MHz, 37 °C, color-coded on the structure. Here the R_{ex} value is defined as $R_{2,eff}$(50 Hz) − $R_{2,eff}$(1000 Hz). Note that R_{ex} can also be negative in cases where substantial $\Delta\varpi_H$ values are obtained (see, for example, Figure 4d), but in all cases in MSG $R_{ex} \geq -2$ s^{-1} (see Supporting Information). Approximately 20% of the methyls studied (46 of 231) have $R_{2,eff}$ values that show a pronounced dependence on CPMG frequency, ν_{cpmg}, with $R_{ex} > 3$ s^{-1} measured at both 600 and 800 MHz. It is likely that an even higher fraction of methyls show exchange, since very small multiple quantum dispersion profiles may not necessarily reflect lack of exchange but rather may result from an exchange process in which nonzero $\Delta\varpi_H$ values lead to decreased profiles. Such a high content of methyls involved in millisecond time scale conformational exchange in MSG indicates a quite remarkable degree of conformational heterogeneity, especially considering that the relative orientation of domains appears to be rigidly fixed in the enzyme (at least in response to ligand binding).[22]

Regions of significant R_{ex} localize primarily to the α/β and barrel domains, as well as to the interface between these two regions (Figure 5b). In the case of the α/β domain, significant exchange contributions to R_2 are observed for V188 and V189 from the βD strand, for L240 and I242 from the βI strand, and for a number of proximal methyls of helices αF and αG and strands βI and βJ. Of note, I260 and V261 of the βJ strand, close to the interface with the barrel domain, also show exchange. Large R_{ex} values are also found for residues in loops connecting α/β and barrel domains.

Methyl groups in the barrel domain that exhibit conformational exchange are mostly located near the extended interdomain surface loops. For example, exchanging residue L128 from the α1 helix is proximal to the mobile α2−βK loop joining α/β and barrel domains and consisting of exchanging side chains I309 and L313. L117 at the start of strand β1 (R_{ex} = 12 s^{-1} at

(33) Tugarinov, V.; Muhandiram, R.; Ayed, A.; Kay, L. E. *J. Am. Chem. Soc.* **2002**, *124*, 10025−10035.
(34) Levitt, M.; Freeman, R. *J. Magn. Reson.* **1978**, *33*, 473−476.
(35) Shaka, A. J.; Keeler, J.; Frenkiel, T.; Freeman, R. *J. Magn. Reson.* **1983**, *52*, 335−338.
(36) Marion, D.; Ikura, M.; Tschudin, R.; Bax, A. *J. Magn. Reson.* **1989**, *85*, 393−399.
(37) Koradi, R.; Billeter, M.; Wüthrich, K. *J. Mol. Graphics* **1996**, *14*, 51−55.

800 MHz; only one of the two methyls could be quantified with confidence) is close to an extended surface loop connecting the N-terminal α-helical clasp and barrel domains, while the side chain of L491 from helix α6 ($R_{ex} = 10\ s^{-1}$) makes contacts with an extended helical region joining barrel and C-terminal domains. Interestingly, methyl groups in proximity to the glyoxylate binding site do not show elevated $R_{2,eff}$ values, with the closest exchanging methyl (V389 in β4) 8 Å away. Finally, the C-terminal domain and the N-terminal α-helical clasp are the least mobile on the millisecond time scale. Of interest, the agreement between measured backbone $^1H-^{15}N$ dipolar couplings and those calculated based on the X-ray structure of the glyoxylate-bound form of MSG is highest for the C-domain,[22] perhaps due to the decreased mobility in this region.

Figure 5c highlights the residues for which backbone amide ^{15}N dispersions[6] with $R_{ex}(800\ MHz) = R_{2,eff}(80\ Hz) - R_{2,eff}(960\ Hz) \geq 5\ s^{-1}$, 37 °C, were observed. We have been conservative in our analysis of the ^{15}N data (as with the ^{13}C profiles) and have only considered dispersions from residues that are not overlapped and for which the sensitivity was sufficiently high that we could accurately fit the curves. It is clear that regions with slow time scale backbone and side-chain dynamics overlap. In particular, there is a concentration of millisecond time scale dynamics in the $\alpha 2-\beta$K loop with both backbone and side chains involved, and this region correlates well with the area of the protein that was found to be the most dynamic on a nanosecond time scale[22] and for which X-ray density was not observed in the gloyoxylate-bound form of the enzyme.[11]

Concluding Remarks

We have presented a simple pulse scheme for monitoring millisecond time scale dynamic processes at side-chain methyl positions in proteins. Results of simulations and experiments on MSG and a test sample of a small protein, protein L, establish the utility of the methodology in the case of applications to highly deuterated, methyl-protonated proteins. Samples can be prepared in a straightforward manner in which Ileδ1 methyl probes are protonated and ^{13}C-labeled and where only one methyl of the pair in Leu/Val is $^{13}CH_3$, using commercially available precursors. In the case of high molecular weight proteins such as MSG, the large sensitivity gains relative to HSQC-based methodology[32] are absolutely critical. However, the experiment is also of utility in applications to smaller proteins. In this case, a combination of ^{13}C single quantum and $^{13}C-^1H$ multiple quantum experiments becomes particularly powerful, since the profiles associated with these different coherences can be quite distinct if $\Delta\varpi_H \neq 0$ (Figure 4d and discussion above). The different functional dependence of $R_{2,eff}$ can be exploited to obtain a more robust measure of the exchange parameters than would be possible from either experiment alone. The high sensitivity of this experiment and the dependence of the resulting dispersion profiles on both $\Delta\varpi_C$ and $\Delta\varpi_H$ make it particularly powerful for the study of a wide range of important biological macromolecules.

Acknowledgment. This work was supported by a grant from the Canadian Institutes of Health Research (C.I.H.R.) to L.E.K. and by funding from AstraZeneca and Syngenta. We thank Dr. C. T. Tan (Isotec, OH) for the custom synthesis of α-keto-isovalerate used as a biosynthetic precursor in this work. D.K. is the recipient of a C.I.H.R. training grant postdoctoral fellowship, and V.T. holds a Human Frontiers Science Program postdoctoral fellowship. V.K. thanks the Natural Sciences and Engineering Research Council of Canada for a postdoctoral fellowship. L.E.K. holds a Canada Research Chair in Biochemistry.

Supporting Information Available: Two tables listing exchange parameters obtained from fits of dispersion data recorded on MSG, 37 °C, at 600 and 800 MHz (PDF). This material is available free of charge via the Internet at http://pubs.acs.org.

JA039587I